



**HAL**  
open science

# ns<sub>2</sub>np<sub>4</sub> (n = 4,5) lone pair triplets whirling in M\*F<sub>2</sub>E<sub>3</sub> (M\* = Kr, Xe): stereochemistry and ab initio analyses

Jean Galy, Samir F. Matar

► **To cite this version:**

Jean Galy, Samir F. Matar. ns<sub>2</sub>np<sub>4</sub> (n = 4,5) lone pair triplets whirling in M\*F<sub>2</sub>E<sub>3</sub> (M\* = Kr, Xe): stereochemistry and ab initio analyses. *Solid State Sciences*, 2017, 64, pp.114-124. 10.1016/j.solidstatesciences.2016.12.004 . hal-01464687

**HAL Id: hal-01464687**

**<https://hal.science/hal-01464687>**

Submitted on 23 Feb 2017

**HAL** is a multi-disciplinary open access archive for the deposit and dissemination of scientific research documents, whether they are published or not. The documents may come from teaching and research institutions in France or abroad, or from public or private research centers.

L'archive ouverte pluridisciplinaire **HAL**, est destinée au dépôt et à la diffusion de documents scientifiques de niveau recherche, publiés ou non, émanant des établissements d'enseignement et de recherche français ou étrangers, des laboratoires publics ou privés.

**SSSCIE 5431** **$ns^2np^4$  ( $n = 4, 5$ ) Lone Pair Triplets Whirling in  $M^*F_2E_3$  ( $M^*=Kr, Xe$ ):  
Stereochemistry and ab initio analyses.**

Jean Galy<sup>1</sup> and Samir F. Matar<sup>2,\*</sup>

<sup>1</sup>CNRS, LCTS, Université de Bordeaux, Pessac. France.

<sup>2</sup>CNRS, ICMCB, Université de Bordeaux, Pessac. France

<sup>2,\*</sup>Corresponding author emails: [Samir.Matar@icmcb.cnrs.fr](mailto:Samir.Matar@icmcb.cnrs.fr) ; [abouliess@gmail.com](mailto:abouliess@gmail.com)

<sup>1</sup>[galy@lcts.u-bordeaux.fr](mailto:galy@lcts.u-bordeaux.fr); [jdgaly@orange.fr](mailto:jdgaly@orange.fr)

**Keywords:**  $ns^2np^4$  electron lone pairs. Solid state stereochemistry. DFT. ELF. DOS

## Abstract

The stereochemistry of  $ns^2 np^4$  ( $n = 4, 5$ ) lone pair LP characterizing noble gas Kr and Xe (labeled  $M^*$ ) in  $M^*F_2$  difluorides is examined within a coherent crystal chemistry and ab initio visualizations.  $M^{*2+}$  in such oxidation state brings three lone pairs (E) and difluorides are formulated  $M^*F_2E_3$ . The analyses use electron localization function (ELF) obtained within density functional theory calculations showing the development of the LP triplets whirling  $\{E_3\}$  quantified in the relevant chemical systems. Detailed ELF data analyses allowed showing that in  $\alpha$ - $KrF_2E_3$  and isostructural  $XeF_2E_3$  difluorides the three E electronic clouds merge or hybridize into a torus and adopt a perfect gyration circle with an elliptical section, while in  $\beta$ - $KrF_2$  the network architecture deforms the whole torus into an ellipsoid shape. Original precise metrics are provided for the torus in the different compounds under study. In  $KrF_2$  the geometric changes upon  $\beta \rightarrow \alpha$  phase transition is schematized and mechanisms for the transformation with temperature or pressure are proposed. The results are further highlighted by electronic band structure calculations which show similar features of equal band gaps of 3 eV in both  $\alpha$ -and  $\beta$ - $KrF_2$  and a reorganization of frontier orbitals due to the different orientations of the F-Kr-F linear molecule in the two tetragonal structures.

## 1- Introduction

A novel approach of lone electron pairs stereo-chemical influence was recently proposed in the crystal networks of chemical compounds [1-2] with the purpose of complementing crystal chemistry analyses with ones carried out within density functional theory (DFT) [3-4] of the electron localization function (ELF) [5-6]. In those works focus was made on post lanthanide  $6s^2$  Tl(I) to Po(IV) in tetrahedral, triangular bipyramidal, square pyramidal, octahedral and hexahedral in different coordinations of chemical compounds (fluorides, oxides and oxyfluorides). Also regarding the implication of electron lone pair E in determining the physical properties, the role played by  $\text{Sn}^{\text{II}}\text{E}$  and  $\text{Pb}^{\text{II}}\text{E}$  in the properties of superionic conductivity of  $\text{PbSnF}_4\text{E}_2$  was further clarified in a recent work [7].

Less encountered class of rare chemical compounds are noble gas (Ng) ones due to the chemical inertness of VIIIA group elements which possess saturated valence shell. However Ng difluorides are known and early works were devoted to their synthesis in special conditions such as the case for  $\text{RnF}_2$ ,  $\text{KrF}_2$  or  $\text{XeF}_2$ . The former,  $\text{RnF}_2$ , obtained by direct interaction of radon and  $\text{F}_2$  shows an intense radioactivity and therefore has been less investigated than Kr and Xe compounds [8].  $\text{RnF}_2$  alike the two other fluorides exhibits a linear conformation F-Rn-F with a bond length  $\text{Rn-F} = 2.08\text{\AA}$ . Both Xe and Kr have shown a large capacity to develop a peculiar chemistry which has been promoted with the investigations of structure determination [9-10]. Also few modeling works were focused on the bonding properties [11-12]. In the context of the present topic the crystal networks of the linear molecules  $\text{RnF}_2\text{E}_3$ ,  $\text{XeF}_2\text{E}_3$ ,  $\text{KrF}_2\text{E}_3$  exhibit –as it is shown in their formulations– the peculiarity of possessing three lone pairs E, whose stereoactivity and steric effects are not known to the best of our knowledge. This is rationalized here in the context of pursuing our former works with further highlighting the electronic localization and structure based on combined crystal chemistry descriptions and computational electronic structures.

## 2- Computational methodology

Within DFT we used the Vienna *ab initio* simulation package (VASP) code [12-14] which allows geometry optimizations with energy minimization. Such procedure is necessary to obtain the ground state electronic structure. From this and for the purpose of analyzing the electron lone pair stereoactivity the electron localization around the chemical constituents

needs to be analyzed. This can be done through different schemes such as the electron localization indicator (ELI-D) [15] or the electron localization function (ELF) used here [5,6]. ELF scheme is based on the kinetic energy in which the Pauli Exclusion Principle is included:  $ELF = (1 + \chi_\sigma^2)^{-1}$  with  $0 \leq ELF \leq 1$ , i.e. it is a normalized function. Then a color scheme follows: in the 2D ELF slice absence of electron localizations corresponds to blue zones, free electron like behavior corresponds to green zones and strong electron localizations are indicated by red zones. In ELF expression the ratio  $\chi_\sigma = D_\sigma / D_\sigma^0$ , where  $D_\sigma = \tau_\sigma - \nabla_s - 1/4 (\nabla \rho_\sigma)^2 / \rho_\sigma$  and  $D_\sigma^0 = 3/5 (6\pi^2)^{2/3} \rho_\sigma^{5/3}$  correspond respectively to a measure of Pauli repulsion ( $D_\sigma$ ) of the actual system and to the free electron gas repulsion ( $D_\sigma^0$ ) and  $\tau_\sigma$  is the kinetic energy density.

For comparing the relative stabilities of the two crystal varieties of  $KrF_2$  and establishing trends of transformation from  $\beta$  to  $\alpha$  phase, subsequent establishment of the energy-volume equations of states EOS, was done based on Birch EOS [16].

Within VASP the projector augmented wave (PAW) method [14, 17] was used to account for explicit atomic configuration (valence/semi-core states) as based on the generalized gradient approximation (GGA) [15] scheme for the effects of exchange and correlation within DFT. In the computational scheme the conjugate-gradient algorithm [19] was used to relax the atoms of the different crystal setups. The tetrahedron method with Blöchl corrections [20] as well as a Methfessel-Paxton [21] scheme was applied for both geometry relaxation and total energy calculations. Brillouin-zone (BZ) integrals were approximated using the special k-point sampling of Monkhorst and Pack [22]. The optimization of the structural parameters was performed until the forces on the atoms were less than  $0.02 \text{ eV/\AA}$  and all stress components less than  $0.003 \text{ eV/\AA}^3$ . The calculations were converged at an energy cut-off of 350 eV for the plane-wave basis set with respect to the k-point integration with a starting mesh of  $6 \times 6 \times 6$  up to  $12 \times 12 \times 12$  for best convergence and relaxation to zero strains.

### 3- Results and discussions

Krypton difluoride  $KrF_2$  is a linear molecule characterized by a particular Lewis dot structure whereby the 8 valence electrons ( $4s^2, 4p^6$ ) arrange as depicted in Fig. 1 with two of them completing the octet around each F and three electron doublets are left non bonding. The

resulting electronic image around Kr is unusual for the chemist as it shows more than eight valence electrons of the well known octet rule. This configuration is termed as “expanded octet”, i.e. 10 electrons, schematically shown in Fig. 1. Corollary to this, Kr compounds are only known with this divalent state. However Xe exists in compounds with tetravalent  $\text{Xe}^{4+}$  ( $\text{XeF}_4$ ) and one may wonder why no compounds with tetravalent Kr are known.

The spatial arrangement of these doublets is little explored or known and its analysis constitutes the major topic of this work besides electronic structure properties. In this representation we note krypton fluoride with its three lone pairs E as:  $\text{KrF}_2\text{E}_3$ ; this also stands for isostructural xenon difluoride,  $\text{XeF}_2\text{E}_3$ .  $\text{KrF}_2$  is a colorless and volatile solid characterized in its linear molecule by  $d(\text{Kr}-\text{F}) \sim 1.9 \text{ \AA}$ . In 1963 Levy and Agron [9] reported on the structure determination of  $\alpha$ - $\text{KrF}_2$ , one form of this difluoride characterized by showing a dimorphism as established by Raman spectroscopy.

The two crystallographic forms  $\alpha$  and  $\beta$  were again investigated in 1972 by Burbank et al. [10] and more recently (2001) refined by Lehmann et al. [23]. In Fig. 2 the linear molecule F-Kr-F can be visually identified with different orientations in the two forms. It can be noted that  $\text{KrF}_2$  and ionized  $\text{KrF}^+$  and  $\text{Kr}_2\text{F}_3^+$  entities were used as complexing materials with  $\text{MF}_6$  (M=As, Sb, Bi) [24].

$\text{XeF}_2$  is likewise a linear molecule and it crystallizes in the tetragonal system as shown by Levy and Agron [9] and more recently refined by Elliot *et al.* [25]. Oppositely to  $\text{KrF}_2$ ,  $\text{XeF}_2$  is only known in  $\alpha$  form.

### 3.1- Krypton difluoride $\text{KrF}_2$

Tables 1 and 2 bring together the crystal data of the two Kr difluorides  $\alpha$  and  $\beta$ . Starting from these data we carried out geometry optimization for subsequent study of electron density and localization and for establishing the energy-volume equation of state (EOS) for determining the ground state structure. The results of the fully relaxed structures are provided in the lower parts of the two tables. They exhibit a good agreement with experiment.

Therefore, before proceeding further, worthy to note that very little attention, even none, was paid to the study of the three lone pairs  $\{\text{E}_3\}$  (called “ $\{\text{E}_3\}$  triplet”) of Kr in the literature.

This is an astonishing lack especially that they obviously surround  $\text{Kr}^{2+}$  cation. According to

VSEPR approach [26] they should be situated, like for example F atoms in  $\text{AsF}_5$ <sup>1</sup> [24], at the apices of equatorial trigonal base in a  $\text{KrF}_2\text{E}_3$  trigonal bipyramid (TBP). Andersson [27], in 1979, pointed out this problem for the isostructural compound  $\text{XeF}_2\text{E}_3$ , the prototype of  $\alpha$   $\text{KrF}_2\text{E}_3$ , suggesting overcoming the constraint of  $\bar{4}$  inversion axis presence along F-Kr-F linear molecule, which does not allow trigonal setting for three E. To do so Andersson proposed {E<sub>3</sub>} triplet to revolve around Kr “with a vortex structure, lone pairs E being smeared out in a ring” then allowing the presence of the two F atoms at TBP axial apices. Worthy to note the volume of  $\text{AsF}_5$  cell for two molecules  $V = 185\text{\AA}^3$ , which corresponds to a reduced volume (rV), i.e. averaged over fluoride constituents:  $rV(\text{F}) = V/10 = 18.5\text{\AA}^3$ , arsenic cation being considered having a negligible volume versus  $\text{F}^-$ . Compared to  $\text{AsF}_3\text{E}$ <sup>2</sup> [29] characterized by a reduced volume  $V(\text{F},\text{E}) = V/8 = 16.7\text{\AA}^3$  (6 F and 2 E) in reasonable agreement with our postulate that E and  $\text{F}^-$  occupy similar volumes in the case of  $ns^2$  lone pairs –cf. [1-2]. With  $\text{KrF}_2\text{E}_3$  molecule, if similar calculation for the reduced volume is done one finds  $rV(\text{F},\text{E}) = V/10 = 11.3\text{\AA}^3$ . This value can be considered as too low, therefore indicating that each lone pair in {E<sub>3</sub>} exhibits a lower volume than  $ns^2$  E. A rough evaluation led to consider only 50% of {E<sub>3</sub>} triplets, then giving for  $Z = 2$   $\text{KrF}_2\text{E}_3$  molecules in the cell  $rV(4\text{F}+\text{only } 3\text{E}) = V/7 = 16.2\text{\AA}^3$ . Therefore it can be assumed that the three  $\text{Kr}^{2+}$  lone pairs do not show individual behavior and they are likely smeared/mixed in a new shape as shown and detailed here below.

This point is supported if we consider the series  $[\text{KrF}]^+[\text{MF}]_6^-$  with  $M = \text{As}, \text{Sb}, \text{Bi}$  which results from  $\text{MF}_5$  and  $\text{KrF}_2$  association via a fluorine bridge. For example  $[\text{KrF}\{\text{E}_3\}][\text{AsF}]_6$  cell volume amounts to  $556.02\text{\AA}^3$  with  $Z = 4$ , i.e.  $139\text{\AA}^3$ , not so far from  $V_{\text{AsF}_5} + V_{\text{KrF}_2\text{E}_3} = 92.5 + 56.7 = 149.2\text{\AA}^3$ . It is obvious, owing to the large value of  $rV_{\text{KrF}_2\text{E}_3}$ , that {E<sub>3</sub>} occupy

<sup>1</sup>  $\text{AsF}_5$ , hexagonal system, space group  $P6_3/mmc$ ; cell:  $a = b = 5.771\text{\AA}$ ,  $c = 6.414\text{\AA}$ ,  $V = 185.0\text{\AA}^3$ ,  $Z = 2$ .  $\text{AsF}_5$  molecule exhibits a perfect trigonal bipyramidal geometry.

<sup>2</sup>  $\text{AsF}_3\text{E}$  orthorhombic system, space group  $Pn2_1a$ ; cell:  $a = 7.018\text{\AA}$ ,  $b = 7.315\text{\AA}$ ,  $c = 5.205\text{\AA}$ ,  $V = 267.2\text{\AA}^3$ ,  $Z = 4$ .  $\text{AsF}_3\text{E}$  molecule shows typical one sided coordination to the three F atoms E being at the apex of  $\text{AsF}_3\text{E}$  tetrahedron. {Note : coordinate of F1  $z = 0.1005$ }.

a large volume indicating its paramount importance in krypton difluoride crystal architecture and its various compounds. Such simple calculation makes sense because in the series  $[\text{KrF}][\text{MF}]_6$  ( $M = \text{As}, \text{Sb}, \text{Bi}$ ), the corresponding reduced volumes calculated according to this proposition are 16.4, 17.5,  $18.2\text{\AA}^3$  respectively; again for  $\beta$  form  $rV_{\beta\text{KrF}_2\text{E}_3} = 17.5\text{\AA}^3$  and for xenon difluoride,  $rV_{\text{XeF}_2\text{E}_3} = 17.8\text{\AA}^3$ .

As indicated above  $\alpha\text{-KrF}_2$  exhibits a linear shape aligned along  $\bar{4}$  axis as shown in Fig. 3a with Kr-F bond around  $2\text{\AA}$ ; this is common to Xe and Kr designated by  $M^*$ . Fig. 3b shows the electronic torus around  $M^{*2+}$  cations. The centers of these F- $M^*$ -F molecules are set up on cell corners and on the center  $\frac{1}{2} \frac{1}{2} \frac{1}{2}$  revolving around F- $M^*$ -F, coiling with the inversion  $\bar{4}$  axis and designing an electronic torus (pale blue color).

The three lone pairs  $\{\text{E}_3\}$  attached to  $M^*$  should then strongly repulse F atoms [28]. Therefore revolving around  $M^*$ , in  $\{\text{E}_3\}$  the three lone pairs E are smeared into the torus allowing ionic attraction  $M^{*2+} \rightarrow \text{F}^-$ . The two F atoms linked to  $M^*$  and the eight Ftp(a to h) of the molecules sited on cell corners form a bicapped tetragonal prism encapsulating  $M^{*2+}$ , therefore  $M^*\text{-Ftp} = 3.248\text{\AA}$  (Kr) and  $3.338\text{\AA}$  (Xe) cannot be retained in  $M^*$  bonding system but only as surroundings of the large  $\{M^*\text{E}_3\}$  unit in a non bonding manner.

Looking at Fig. 3b the question of lone pair size emphasized by the  $\{\text{E}_3\}$  triplet revolution around Kr or Xe becomes obvious and there is a need to settle it:

- \* Firstly in order to prove and define it in agreement with the real F and  $\{\text{E}_3\}$  volumes which occupy the cells;
- \* Secondly to define their architecture and extend the determination of their chemical and physical influences in the various compounds.

### ***Electron localization function of $\alpha\text{-KrF}_2$***

Such crystal chemistry task is made possible with joint help from accurate determination of the electron localization (EL) around the atoms with DFT calculations of the electron localization function ELF introduced above with three and two dimensional (3D and 2D) mappings. This especially pertains for the proof of existence of such  $\{\text{E}_3\}$  lone pairs and their illustrations and geometric specifications of shape, size and volumes as developed hereafter.

Figure 4 shows ELF projections of  $\text{KrF}_2$  with 3D (grey volumes) and 2D (slices with color code following the introduction above). In these views it is important to note that effectively the three lone pairs  $\{E_3\}$  are revolving around Kr atom in the median plane of F-Kr-F molecule designing a perfect electronic torus. Note that apical fluorine atoms F show also a ring of density around F-Kr-F axis, indicating that their electrons are swept along by  $\{E_3\}$  triplet whirling. In  $\{E_3\}$  torus it is reasonable to postulate that the three E's would be separated by  $120^\circ$  angle –were they to be described individually–. The 2D slices show that electrons are found within the F-Kr-F molecular entities with strong localization around F and Kr-E3. The bonding between Kr and F is signaled by weak yellow ELF exhibiting bonding, likely ionic due to the chemical nature of F (highest electronegativity element).

To understand ELF sections, the analyses of  $\text{KrF}_2E_3$  pertinent data are documented in Table 2 and their representation are given in Figure 5.

ELF section at Fig. 5a, parallel to (001) and perpendicular at Kr to the fourfold axis, shows the median plane of  $\{\text{KrE}_3\}$  part of the molecule. The second panel (Fig. 5b) in lower part, right in (110) plane, contains the linear F-Kr-F molecule and fluorine atoms  $\text{Ftp}(\text{dhbf})$ ; such plane makes a perfect section cut of  $E_3$  torus as evidenced in Fig. 5b. After isolocalization curve (IDC), driving the circular traces generated by  $\{E_3\}$  motion is highlighted.  $\{\text{KrE}_3\}$  forms a perfect circle well separated from the neighbors of next cells, IDC circle with 0.5 isosurface limiting it. The diameter size of the torus designed by E rotation is limited by the white brackets  $0.5 > T < 0.5$  in between 0.5 IDC; its measured value is  $T = 1.32\text{\AA}$ . These values allow defining the gyration radius  $r_{E\_gyr}$  of  $E_3$  torus,  $r_{E\_gyr} = (\varnothing_{\text{Text}} - T) / 2 = 0.78\text{\AA}$ ; it is indicated in the figure by a yellow circle which is also the locus of E centers of each lone pair cloud assimilated to electronic sphere (white transparent circles) having a radius  $r_E = T / 2 = 0.66\text{\AA}$ . This yellow circle sits in the middle of the highest electronic density ring (IDC  $> 0.90$ ) delimited by green brackets. Owing to the narrow size of this ring both E and Ec locus circuits are supposed to coil onto yellow circle, also marked by green dotted points.

Fig. 5b brings another important feature concerning the shape of E which shows an elongation along [001] indicating that it exhibits an elliptic section. If  $a = b = 0.66\text{\AA}$  in the section parallel to (001) plane, the third parameter of E ellipsoid is  $c = 0.75\text{\AA}$  along [001]. Such data correspond to an average sphere of influence  $r_{E\_Kr} = 0.69\text{\AA}$ .

Following this evolution it was important to appreciate the physical effect relating this  $\alpha$  form tetragonal structure  $I4/mmm$  to another network crystallizing in the same system, the  $\beta$  form of  $\text{KrF}_2\text{E}_3$ , crystallizing in a different space group:  $P4_2/mnm$ .

### 3.2– $\beta\text{-KrF}_2\text{E}_3$ and the phase transition $\beta \rightarrow \alpha$

The linear F-Kr-F molecule in the  $\alpha$  and  $\beta$  forms shows very close bond values Kr-F = 1.897Å ( $\alpha$ ) and 1.886Å ( $\beta$ ). With ab initio calculations d(Kr-F) increases up to 1.935Å while remaining the same for  $\beta$  i.e. 1.887Å (Table 2). Therefore their different packing leads to a completely different fluorine environment around Kr atom. It was shown in preceding paragraph that Kr, within  $\alpha$  phase, is enclosed in a large bicapped tetragonal prism (bTP), eight F coming from neighboring molecules with rather large Kr-F(a...h) = 3.248Å interatomic distances; the fluorine atoms directly linked to Kr are settled at the two capping apices, then one counts altogether 10 F environing Kr.

In the  $\beta$  phase the fluorine polyhedron shows, like in the  $\alpha$  form, 8 apices plus the 2 F of the F-Kr-F linear entity. Therefore this polyhedron with again 10 F in the vicinity of Kr is slightly more complicated to describe (Fig. 6). In a first approach one may notice the 4 F(abcd) designing a rectangle parallel to [001], perpendicular to F-Kr-F and framing  $\text{KrF}_2$ . These fluorine atoms pertain to the  $\text{KrF}_2$  molecules centered on corner cell. Kr-Fabcd = 3.214Å and Fa-b = Fc-d = 2.712Å these four F with the two F linked to Kr design a distorted octahedron:  $\text{KrF}_2\text{Fabcd}$  which shows an elongated rectangular equatorial plane with an elongation along [001] amounting to Fa-d = Fb-c = 5.827Å. These  $\{\text{KrF}_6\}$  distorted octahedra are organized exactly like  $\text{TiO}_6$  octahedra in the rutile-like structure, i.e. endless files of edge sharing  $\{\text{KrF}_6\}$  octahedra via Fa-b and Fc-d coiled along  $\bar{4}$  axis and connected by F apices.

Important also to note in the plane parallel to (001) containing the molecule  $\text{KrF}_2$  (in  $\frac{1}{2}, \frac{1}{2}, \frac{1}{2}$ ), the presence of four extra fluorine atoms F<sub>m,n,o,p</sub> with Kr-F<sub>mnp</sub> = 3.514Å in the four neighbor (100) and (010) face shared cells. They complete the fluorine  $\{\text{KrE}_3\}$  surrounding up to 10.

The volume of this polyhedron encapsulating  $\{\text{KrE}_3\}$  amounts to  $60.2\text{Å}^3$ . It corresponds to  $\text{F}_2\text{Fabcd}$  octahedron volume  $19.6\text{Å}^3$  plus the two octahedra  $\text{F}_a(\text{FF}_{\text{op}}\text{F})\text{F}_d$  and  $\text{F}_b(\text{FF}_{\text{mn}}\text{F})\text{F}_c$

with volumes  $20.3\text{\AA}^3 \times 2$ . A schematic view along [001] to visualize this  $\{\text{KrE}_3\}$  shaping is shown in Fig. 7. Compared with the corresponding volume of the bicapped tetragonal prism in the  $\alpha$  form  $53.5\text{\AA}^3$  one may note a 12.5% increase, which is larger than single crystal cell volume expansion 8.1%.

This drastic difference in the shaping volume of  $\alpha$ - and  $\beta$ -  $\text{KrF}_2\text{E}_3$  molecules, while Kr-F and F-F distances are not so different, lets us suppose that *something* happens in the rearrangement of the three lone pairs revolving around Kr atom. Therefore it allows a molecular packing change with comparable resulting reduced volume, around  $17\text{\AA}^3$ , for both  $\alpha$  and  $\beta$  phases.

### ***Electron localization function of $\beta$ $\text{KrF}_2$***

ELF calculations were subsequently performed. We focus on the cross sections (2D ELF) of the data allowing to precise  $\{\text{KrE}_3\}$  torus evolution (Fig. 8 a,b,c).

A section plane containing Kr and Fabcd fluorine atoms allows visualizing the shape of the Kr and E3 torus of  $\text{KrF}_2$  molecule in  $\beta$  form (Fig. 8a). It is worth noting a drastic difference with  $\alpha$ - $\text{KrF}_2$   $\{\text{KrE}_3\}$  showing an elliptical distortion induced by an ionic repulsion of Fabcd fluorine atoms. The previous circular form is flattened in the axis of these four fluorine atoms inducing a long expansion of the torus along [110] in the large free angular space defined by  $\angle \text{FaKrFd}$  and  $\angle \text{FbKrFc}$  angles which does not show any strong barrier, and perpendicular (between  $\angle \text{FaKrFb}$  and  $\angle \text{FcKrFd}$  angles) a limited bulge in [001] direction braked by the narrow size of Fabcd rectangle. The result of such deformation gives a clear ellipsoidal form to  $\{\text{KrE}_3\}$  torus. Then the three lone pairs revolve along an elliptic locus (yellow color) whose maximum density curves design plots above  $\text{IDC} > 0.93$ .

The maximum ring, in between  $\text{IDC} = 0.92$  ellipses, is narrower than in  $\alpha$ - $\text{KrF}_2$ . So the ellipse; locus of lone pair centroid  $E_c$  (green) and of E center of electronic volume of influence (yellow) are quasi coiled. The two sections in Fig. 8b and 8c allow precisizing the thickness of the torus which is directly related with the size of lone pair electronic clouds; these are not spherical but slightly elongated along [001] forming a kind of ellipsoid. When E electronic clouds are running along the yellow ellipse in (001) plane their plasticity allows to

adapt them to the elliptical shape of the torus while their height remains on the whole similar as shown by Fig. 8b and 8c, i.e.  $H = 0.8\text{\AA}$ . External shape of these toruses (same figures) is limited by a rounded rectangle (red line) with  $L = 3.2\text{\AA}$  along  $[110]$  and  $2.8\text{\AA}$  along  $[110]$  alike in the (001) plane Fig. 8a). The ellipsoid of E cloud then shows a height given by H, c parameter is equal to  $0.8\text{\AA}$ , while its 'a' and 'b' axes range between  $0.79$  and  $0.88\text{\AA}$  when E runs along the yellow circle. All pertinent distances are summarized in Table 2.

### 3.3 Mechanism of the phase transition $\beta \rightarrow \alpha$ upon lowering temperature (or increasing pressure).

$\beta$ - $\text{KrF}_2\text{E}_3$  phase according to its authors was distilled and crystallized at low temperature. Such type of protocol could favor the creation of the distorted surrounding of  $\{\text{KrE}_3\}$  and eventually to the distortion of its shape. Therefore the phase transition which results in  $\alpha$   $\text{KrF}_2\text{E}_3$  occurs without disruption, suggesting a simple atomic rearrangement to obtain the  $\beta \rightarrow \alpha$  transformation. A proposal is illustrated in Fig. 9a,b,c where  $\text{KrF}_2$  molecules in alternate planes parallel to (001) rotate clockwise and anticlockwise.

After  $90^\circ$  rotation all the molecules become aligned in a unique direction and  $\alpha$ - $\text{KrF}_2\text{E}_3$  phase is obtained (Fig. 9c). Then the cloud of lone pairs in their *ballet* around Kr having the largest space of the symmetric bicapped tetragonal fluorine prism can run in a perfect circle stabilizing the  $\alpha$  phase. During these rotations, the tetragonal parameter  $c_\beta = 5.827\text{\AA}$  increases up to  $c_\alpha = 6.5047\text{\AA}$ , while the packing between the layers containing  $\{\text{KrE}_3\}$  ( $1\bar{1}0$ ) and (110) becomes more efficient; then  $a_\beta$  becomes  $a_\alpha$ . So the cell orientation is preserved and  $(a,b,c)_\beta \rightarrow (a,b,c)_\alpha$  transformation should consume little energy. This mechanism is slightly different from the one proposed in [24] which leads to  $a_\beta \rightarrow c_\alpha$ ,  $b_\beta \rightarrow a_\alpha$  and  $c_\beta \rightarrow b_\alpha$ .

We also show that such transformation can be induced by pressure by establishing the respective energy volume equations of state.

### 3.4 Energy-volume equation of state EOS

For both compounds the agreement with starting experimental data (Table 1 and 2) is good enough to examine their relative energy/volume behaviors and physical properties such as the bulk modulus

derived from the energy-volume equation of state (EOS). This is obtained from the least squares fit of the energy/volume curves  $E$  versus  $V$  using the Birch equation of state EOS up to the 3<sup>rd</sup> order [16]:

$$E(V) = E_0 + \frac{9}{8} B_0 V_0 \left[ \left( \frac{V_0}{V} \right)^{\frac{2}{3}} - 1 \right]^2 + \frac{9}{16} B_0 (B_0' - 4) V_0 \left[ \left( \frac{V_0}{V} \right)^{\frac{2}{3}} - 1 \right]^3$$

where  $E_0$ ,  $V_0$ ,  $B_0$  and  $B_0'$  are respectively the energy and volume at equilibrium, the zero pressure bulk modulus and its pressure derivative. The obtained values are given in the inserts of Fig. 10 showing the energy-volume curves. The fit curves reproduce the trends of the geometry optimization for the volume with a small deviation.

$\beta$ -KrF<sub>2</sub> is clearly identified as a ground state phase in as far as it is found at larger volume and lower energy versus  $\alpha$ -KrF<sub>2</sub> at smaller volume and higher energy. The relative magnitudes of the bulk moduli  $B_0$  follow from this, i.e.  $\alpha$  KrF<sub>2</sub> characterized by smaller volume is less compressible than  $\beta$  KrF<sub>2</sub>. This agrees for the volume change with experimental observation (cf. Tables 1 and 2). Then it can be assumed that this low temperature form can also be accessed by exerting an external pressure.

### 3.5- Electronic band structures and site and l-projected density of state (DOS).

We discuss the electronic band structures and site projected DOS of  $\alpha$  and  $\beta$ -KrF<sub>2</sub> in order to provide further understanding of the differences between them especially as regarding the reorientation of the linear F-Kr-F molecule in the two phases.

Fig. 11 a) and b) shows the band structure plotted along the major directions of the tetragonal Brillouin zone (BZ) for  $\alpha$  and  $\beta$ -KrF<sub>2</sub>.

In panels a) and b) as well as on other plots of Fig. 11 the zero of energy is with respect to  $E_v$ , top of the valence band (BV) which is separated from the conduction band (CB) by a band gap of  $\sim 3$  eV pointing out to insulating behavior of both varieties<sup>3</sup>. The overall shape of the bands both in VB and CB is similar in both panels with the difference of twice larger number of bands in the  $\beta$  form due to twice larger number of atomic constituents (2 formula units FU per cell, P centering) versus  $\alpha$ -KrF<sub>2</sub> (one FU explicitly accounted due to the body centered I centering). There are two main blocks of bands in the VB, at  $\sim -6$  eV for s-like states (due to

---

<sup>3</sup> Note that band gaps within DFT different exchange-correlation functionals are not to be considered as exact ex. versus experiment; the given value is only to be taken as indicative here.

Kr, knowing that F-s states, much deeper in energy are not shown here) and in the range  $\{-4\text{eV}-E_V\}$  for p block states. More details are obtained from the site projected DOS (PDOS in c and d panels) as well as from the projections of the *p*-orbitals of Kr in panels c and e.

The PDOS also show similar general shapes especially for the Kr s states mixing with F at -6 eV and the prevailing large intensity F-p states mixing with Kr valence states mainly at  $\sim -4$  eV and less bonded with Kr from -4 eV up to  $E_V$ . Due to the different orientations of the linear F-Kr-F in the two structure differences can be expected upon decomposing the Kr valence states onto *l* components. This is exhibited in Figs 11 d) and f) for  $\alpha$  and  $\beta$ -KrF<sub>2</sub> respectively. Differences are indeed observed for such projections mainly for  $\alpha$ -KrF<sub>2</sub> with the stabilization at low energy of Kr-*p<sub>z</sub>* oriented along linear F-Kr-F and the *c*-tetragonal axis where opposite features are observed for  $\beta$ -KrF<sub>2</sub> where the *p<sub>x,y</sub>* are now stabilized at -6 eV and the Kr-*p<sub>z</sub>* destabilized towards -4 eV and at the top of VB. Similar opposite features are observed within the CB where the lowest unoccupied states (similarly to LUMO in molecular orbitals terminology) are identified as *p<sub>z</sub>* and *p<sub>x,y</sub>* respectively in  $\alpha$  and  $\beta$ -KrF<sub>2</sub>. Consequently the phase transition  $\beta \rightarrow \alpha$ , while occurring with similar band gap magnitude, exhibits significant rearrangements of the states at the VB top and CB bottom; or in molecular description, of the HOMO/LUMO orbitals.

Lastly we note that XeF<sub>2</sub> bands and DOS show close resemblance with  $\alpha$ -KrF<sub>2</sub>. Consequently we focus on the discussion of differences with respect to Kr case mainly for the ELF characteristics.

#### 4- Xenon difluoride XeF<sub>2</sub>E<sub>3</sub>

XeF<sub>2</sub> crystallizes in the tetragonal system as F-Xe-F linear molecules, space group *I4/mmm*, as shown from a single crystal neutron diffraction study in 1963 [9]. More recently in 2010 the crystal structure was refined using X-ray data collected at 100K (Table 3) [2]. Important to note that owing to the electronic structure of Xe<sup>2+</sup>, [Kr]4d<sup>10</sup>5s<sup>2</sup>5p<sup>4</sup>, there are also three lone pairs (E), formally written for the compound by XeF<sub>2</sub>E<sub>3</sub> formula; it is the prototype of KrF<sub>2</sub>E<sub>3</sub>.

Crystal structure determination shows that the symmetric linear molecules  $\text{XeF}_2$  are aligned onto inversion  $\bar{4}$  axis along [001] direction. A question of paramount importance comes related to what happens to the three lone pairs ( $E_3$ ) attached to  $\text{Xe}^{2+}$  electronic structure  $[\text{Kr}]5d^{10}5s^25p^4$ . Alike for  $\alpha\text{-KrF}_2E_3$  they should be around Xe in the median plane perpendicular to F-Xe-F. Therefore to overcome  $\bar{4}$  inversion axis presence unsuitable for threefold symmetry of three lone pairs, the Andersson's suggestion [4] was followed: the proposal, indicated as soon as 1979, indicates that the three lone pairs E are packed and revolved in a ring around  $\text{Xe}^{2+}$ . The resulting torus was assimilated to a vortex.

The description of the crystal structure is exactly the same as  $\text{KrF}_2E_3$  one. The three lone pairs ( $E_3$ ) attached to Xe should then strongly repulse F atoms [4]. Therefore, revolving around Xe, the three lone pairs ( $E_3$ ) are smeared into the torus allowing ionic attraction  $\text{Xe}^{2+} \rightarrow \text{F}^-$ ; this bonding is larger than in Kr phase with  $\text{Xe-F} = 1.999\text{\AA}$  instead of  $\text{Kr-F} = 1.897\text{\AA}$  as well as  $\text{Xe-F}_{\text{tp}} = 3.338\text{\AA}$  longer than  $\text{Kr-F}_{\text{tp}} = 3.248\text{\AA}$ <sup>3</sup>. The bicapped tetragonal prism  $\text{F}_2\text{F}_{\text{tp}}\text{a...h}$  encapsulating  $\{\text{XeE}_3\}$  shows then a volume  $V = 65.1\text{\AA}^3$  considerably higher (+22%) than  $\text{KrF}_2E_3$  one i.e.  $53.5\text{\AA}^3$ .

Looking at Fig. 12 the question of lone pair size emphasized by the  $E_3$  triplet revolution around Xe imposes settling  $E_3$  definition in agreement with the real F and cell volumes and to appreciate this evolution as function of the increase of Z atomic number from Kr to Xe.

As above in the case of  $\alpha\text{-KrF}_2$ , based on high precision calculations, the obtained ELF are firstly used to produce the three dimensional 3D isosurface shown in Fig. 12 in a view perpendicular to [001]. It shows immediately that the concept of  $E_3$  making an electronic cloud torus around Xe is confirmed. Then a detailed analysis of ELF view shows new features of the rounded rectangle parameters framing a torus shape section view along [010] direction. The measured parameters are  $L = 3.3\text{\AA}$ ,  $H = 1.8\text{\AA}$  and  $R = 0.92\text{\AA}$  (traced red color line). This L value corresponding to external diameter of  $E_3$  torus is extremely important because it confirms its bigger size than in Kr phase. This indicates again the paramount role of the lone pair triplet in  $\text{XeF}_2$  molecular structure.

Projections with various isocalization sections (similar to Fig. 5a) reveal on the torus gyration circle the variations of the size of the most intense isocalization plots ( $IDC > 0.95$ ). During the revolving the three LP's, separated by  $120^\circ$ , upon passing through  $[110]$  or  $[\bar{1}\bar{1}0]$  planes, right in the rectangular plane of the four Ftp(bfhd) or Ftp(acge), the lone pairs (E) undergo repulsion from Ftp's s. This drives their acceleration leaving a narrow isocalization islet. By corollary when in between these planes E's find an empty space a larger mark of electronic density is left.

### *Sections in electronic localization ELF data.*

In Fig. 13 two sections of ELF data, the former (Fig. 13a) parallel to (001) and perpendicular in Xe to fourfold axis, shows the median plane of  $\{XeE_3\}$  system of the molecule and the second (Fig. 13b) in lower part, right in (110) plane contains the linear F-Xe-F molecule and the fluorine atoms Ftp(dhbf). Such plane makes a perfect section cut of  $E_3$  torus as evidenced in this Fig. 5b.

After isocalization curve (IDC) plotting Fig. 13a shows the circular traces generated by  $\{E_3\}$  spinning around Xe.  $\{XeE_3\}$  forms a quasi perfect circle well separated from the neighbors of next cells, IDC circle with 0.5 value limiting it. The external diameter amounts to  $\varnothing_{Text} = 3.30\text{\AA}$ . The diameter size of the torus designed by  $E_3$  rotation is limited by the white brackets  $0.5 > T < 0.5$  in between 0.5 IDC; its measured value  $T = 1.40\text{\AA}$ . These values allow defining the gyration radius  $r_{Egyr}$  of  $E_3$  torus,  $r_{Egyr} = (\varnothing_{Text} - T) / 2 = 0.95\text{\AA}$ ; it is indicated in the figure by a yellow circle which is also the locus of E centers of each lone pair assimilated to electronic sphere (white transparent circles) having a radius  $r_E = T / 2 = 0.70\text{\AA}$ . Worthy to note that, separated by  $120^\circ$  angle, they exhibit large spacing on this "circuit". Yellow circle is in between two circles corresponding to 0.94 IDC delimitating a ring, size shown by green brackets, containing island of the highest localization, above  $IDC > 0.95$ . Alike in the 3D ELF views it is noted that these electronic densest islands are very small in vicinity of (110) and  $(\bar{1}\bar{1}0)$  plane sections. It is supposed that these concentrated densities indicate the best probability also for lone pair centroid Ec locus revolving along green circle with radius equal to  $Xe-Ec = 0.98\text{\AA}$ .

Fig. 13b brings another important feature concerning the shape of E which shows an elongation along [001] indicating that it exhibits an elliptic section. If  $a = b = 0.70\text{\AA}$  in the section parallel to (001) plane the third parameter of E ellipsoid  $c = 0.92\text{\AA}$  along [001]. Such data correspond to an average sphere of influence  $r_{E\_Xe} = 0.77\text{\AA}$ .

### 5- Molecular calculations on the NgF<sub>2</sub> (Ng=Kr, Xe, Rn) molecules

In as far as the molecular linear entity F-Ng-F has been in the background of our solid state investigations, it becomes relevant to examine it throughout the Ng series under consideration. Also the Rn difluoride molecule was added for the sake of completeness. Calculations with the Gaussian molecular code *G09* [30] were carried out. After different geometry optimization tests aiming at approaching the experimental Ng-F distances, SDD ECP basis set [31] with gradient PBE [18] DFT exchange-correlation functional led to the best results.

Table 4 brings together the results of the molecular calculations. RnF<sub>2</sub> was added for the sake of completeness. The Ng-F distances obtained after geometry relaxation are in agreement with the experimental data in above tables and their increase within the Ng series is in accordance with the increase of the Ng size with the atomic number.

There are 3 frequencies identified in the IR/Raman spectra obtained after geometry relaxation: two IR-active for F–Ng–F bending mode on one hand and for antisymmetric stretching on the other hand; one active mode in Raman corresponds to symmetric F–Ng–F stretching. The frequencies show inversely proportional evolution versus distances, i.e. the larger the interatomic distance, the smaller the frequency. This could be expected in as far as the interatomic distance can be assimilated to a string with force constant proportional to its length. This study provides original illustration of the linear F-Ng-F properties at molecular level.

### 6- Conclusion

In this work we have proposed a new vision of  $ns^2np^4$  ( $n = 4, 5$ ) lone pair LP stereochemistry characterizing noble gas elements Kr and Xe (labeled M\*) in M\*F<sub>2</sub> difluorides. The LP study through coherent crystal chemistry and ab initio electron localization (ELF) clearly shows that divalent M\* brings three lone pairs LP arranging into triplets which form a torus. Particularly in  $\alpha$ -(Kr,Xe)F<sub>2</sub>E<sub>3</sub> difluorides the E<sub>3</sub> electronic torus clouds adopt a perfect gyration circle

with an elliptical section due to E ellipsoid shape. On another hand in  $\beta$ -KrF<sub>2</sub> the network architecture deformed the whole torus in an ellipsoid shape. The mechanism of  $\beta \rightarrow \alpha$  transition with T or P is schematized.

In the calculation of the reduced volume  $r_v$  (cell volume divided by the number of F and E) it is noticed that the average sphere of influence of lone pair is 50% less than E for  $ns^2$  elements like Pb<sup>2+</sup> and Bi<sup>3+</sup>. This could be due to the merging of the three E's into the torus analyzed throughout the paper.

These precisions concerning {E<sub>3</sub>} triplets strongly demonstrate that chemical, structural and physical properties of phases containing elements whose electronic configurations induce their presence cannot be well understood without taking into account their important and remarkable stereochemistry. If Kr<sup>2+</sup> and Xe<sup>2+</sup> constitute a first model, phases with “Br<sup>+</sup>” and “Cl<sup>+</sup>” must also show the same peculiarities.

Further studies are underway.

## References

- [1] Matar S.F., Galy J., Progress in Solid State Chem., 2015, 43, 82-97 [account]
- [2] Galy J., Matar S.F., Progress in Solid State Chem., 2016, 44, 35-58 [account]
- [3] Hohenberg, P.; Kohn, W. Phys. Rev. B 1964, 136, 864
- [4] Kohn, W.; Sham, L. J. Phys. Rev. A, 1965, 140, 1133.
- [5] Becke A.D., Edgecombe K.E., J Chem Phys; 1990, 92, 5397.
- [6] Savin A., Jepsen O., Flad J., Andersen O.K., Preuss H., von Schnering H.G., Angew. Chem. Int Ed Engl, 1992, 31, 187.
- [7] Matar S.F., Galy J., Solid State Sciences, 2016, 52, 29.
- [8] Fields P. R., Stein L., Zirin M. H., J .Amer. Chem. Soc., 1962, 84 [21], 4164.
- [9] Levy H.A., Agron P.A., J .Amer. Chem. Soc., 1963, 85, 241.
- [10] Burbank R.D., Falconer W.E., W.A. Sunder, Science, 1972, 178, 1285.
- [11] Mitchell K.A.R., J. Chem. Soc. [A], 1969, 54, 1637-1644.
- [12] Jones G.R., Burbank R.D., Bartlett N., 1970, Inorg. Chem., 9, 2264.
- [13] Kresse G., Furthmüller J., Phys Rev B, 1996, 54, 11169.
- [14] Kresse G., Joubert J., Phys Rev B, 1999, 59, 1758.
- [15] Wagner F.R., Bezugly V., Kohout M., Grin Y., Chemistry Eur. J. 2007, 13, 5724.
- [16] Birch F., J. Geophys. Res. 1978, 83, 1257.
- [17] Blöchl P. E., Phys Rev B, 1994, 50, 17953.
- [18] Perdew J., Burke K., Ernzerhof M., Phys. Rev. Lett., 1996, 77, 3865.
- [19] Press W.H., Flannery B.P., Teukolsky S.A., Vetterling W.T., Numerical Recipes, Cambridge University Press, New York [1986).
- [20] Blöchl P. E., Jepsen O., Andersen O. K., Phys. Rev. B, 1994, 49, 16223.
- [21] Methfessel M., Paxton A.T., Phys. Rev. B, 1989, 40, 3616.
- [22] H.J. Monkhorst, J.D. Pack, Phys. Rev. B, 1976, 13, 5188.
- [23] Lehmann J.F., Dixon D.A., Schrobilgen G. J., Inorg. Chem., 2001, 40, 3002.
- [24] Koehler J., Simon A., Hoppe R., Z. Anorg. Allg. Chemie, 1989, 575, 55.
- [25] Elliot H.S.A., Lehmann J.F., Mercier H.P.A., Jenkins H.D.B., Schrobilgen G.J., Inorg. Chem., 2010, 49(18), 8504.
- [26] Gillespie R. J., Hargittai I., "The VSEPR Model of Molecular Geometry", Allyn and Bacon, p.149 (1991).
- [27] Andersson S., Acta Cryst. B, 1979, 35, 1321.
- [28] Galy J., Enjalbert R., J. Solid State Chem., 1982, 44, 1.

[29] Andersson S., Aström A., "Solid State Chemistry" Proc. 5<sup>th</sup> Material Research Symposium, p3-13, NBS special publication 364, (1972).

[30] Gaussian 09, Revision D.01, Frisch, M. J.; Trucks, G. W.; Schlegel, H. B.; Scuseria, G. E.; Robb, M. A.; Cheeseman, J. R.; Scalmani, G.; Barone, V.; Mennucci, B.; Petersson, G. A.; Nakatsuji, H.; Caricato, M.; Li, X.; Hratchian, H. P.; Izmaylov, A. F.; Bloino, J.; Zheng, G.; Sonnenberg, J. L.; Hada, M.; Ehara, M.; Toyota, K.; Fukuda, R.; Hasegawa, J.; Ishida, M.; Nakajima, T.; Honda, Y.; Kitao, O.; Nakai, H.; Vreven, T.; Montgomery, J. A., Jr.; Peralta, J. E.; Ogliaro, F.; Bearpark, M.; Heyd, J. J.; Brothers, E.; Kudin, K. N.; Staroverov, V. N.; Kobayashi, R.; Normand, J.; Raghavachari, K.; Rendell, A.; Burant, J. C.; Iyengar, S. S.; Tomasi, J.; Cossi, M.; Rega, N.; Millam, M. J.; Klene, M.; Knox, J. E.; Cross, J. B.; Bakken, V.; Adamo, C.; Jaramillo, J.; Gomperts, R.; Stratmann, R. E.; Yazyev, O.; Austin, A. J.; Cammi, R.; Pomelli, C.; Ochterski, J. W.; Martin, R. L.; Morokuma, K.; Zakrzewski, V. G.; Voth, G. A.; Salvador, P.; Dannenberg, J. J.; Dapprich, S.; Daniels, A. D.; Farkas, Ö.; Foresman, J. B.; Ortiz, J. V.; Cioslowski, J.; Fox, D. J. Gaussian, Inc., Wallingford CT, 2009. (Licence University of Bordeaux).

[31] Fuentealba P., Preuss H., Stoll H., Szentpály L. V., "A Proper Account of Core-polarization with Pseudopotentials - Single Valence-Electron Alkali Compounds," Chem. Phys. Lett., 1982, 89 418.

## Tables

Table 1 - Crystal and DFT data for  $\alpha$   $\text{KrF}_2\text{E}_3$ .

$\alpha$ - $\text{KrF}_2\text{E}_3$ - Tetragonal, Space group $I4/mmm$ (N°139) - 100K								
		a (Å)	b (Å)	c (Å)	V (Å <sup>3</sup> )	Z	rV(F,{E3})(Å <sup>3</sup> )	
Crystal [25]		4.1744	4.1744	6.5047	113.35	2	16.2	
DFT-ELF		4.1808	4.1808	6.5912	115.21	2	16.5	
<i>Interatomic distances (Å) - 1) crystal - 2) ab initio relaxed geom. and ELF analyses</i>								
1)	Kr-F	1.897	Kr-Ftp	3.248	F-Ftp	3.001	Ftp high	2.710
	Kr-E	0.85	F-E	2.23	Ftp-E	2.82		
2)	Kr-F	1.935	Kr-Ftp(x8)	3.254	F-Ftp	3.012	Ftp high	2.721
	Kr-Ec	0.78	Kr-E	0.78	Ec-E	0.06	E ellipsoid a/b/c	0.66/0.66/0.75
	F-Ec	2.09	Ftp-E	2.82				
	>T<	1.32	∅Text	2.88	rTgyr	0.78	T.rd.rect. L/H/R	2.84/1.5/0.8

>T<: E torus diameter in median plane containing the three lone pairs. ∅Text and rTgir: E torus external diameter and gyration radius. T.rd.rect.: torus rounded rectangle encapsulating E torus section generated by E<sub>3</sub> revolving around Kr. Ec is the locus of lone pair centroid.

Ftp: fluorine atoms making the tetragonal prism around Kr. Ftp high: high of tetragonal prism.

rE = (a.b.c)<sup>1/3</sup> = 0.69Å: average sphere of influence radius of each lone pair.

Table 2 - Crystal and DFT data for  $\beta$   $\text{KrF}_2\text{E}_3$ .

$\beta$ $\text{KrF}_2\text{E}_3$	Tetragonal, Space group $P4_2/mnm$ (N°139) - 193K.					
	a (Å)	b (Å)	c (Å)	V (Å <sup>3</sup> )	Z	rV(F,{E3})(Å <sup>3</sup> )
Crystal [25]	4.585	4.585	5.827	122.50	2	17.5
DFT-ELF	4.585	4.585	5.805	115.03	2	16.4

***Interatomic distances (Å) - 1) crystal - 2) ab initio relaxed geom. and ELF analyses***

1)	Kr-F	1.886	Kr-Fabcd	3.214	Kr-Fmnop	3.514	Rect. plane (abcd) l x h	2.712 x 5.827
	Kr-E	0.79 - 0.88	F-Eax	2.03	F-Eeq	2.06	Rect. plane (mnop) l x h	2.712 x 6.484
2)	Kr-F	1.887	Kr-Fabcd	3.203	F-Fmnop	3.514	Oct. eq rect. l x h	2.710 x 5.805
	Kr-Ec	0.79 - 0.88	F-Eax	2.08	F-Eeq	2.05	E ellipsoid (a/b/c) yellow	0.88/0.79/0.80
	>.T.<	1.32	ØTextax	3.15	ØText eq	2.78	T.rd.rect.L/H/R	3.0-2.7/1.5/0.8

> T <: E torus ellipse in median plane (between IDC = 0.92) (cf. Fig. 5) containing the three lone pairs revolving along yellow-green ellipse. ØText.ax and φText.eq: E torus external dimensions. T.rd.rect.: torus rounded rectangle encapsulating E torus sections perpendicular to median plane with extreme values along [110] and [001]. F-Eax towards [001]; F-Eeq towards [110].

Fabcd: equatorial rectangle plane of  $\text{KrF}_6$  octahedron; F at apices.

rE = (a.b.c)<sup>1/3</sup> = 0.82Å: average sphere of influence radius of each lone pair.

Table 3 - Crystal [25] and DFT data for XeF<sub>2</sub>E<sub>3</sub>.

XeF <sub>2</sub> E <sub>3</sub> - Tetragonal, Space group <i>I4/mmm</i> (N°139) - 100K.								
	a (Å)	b (Å)	c (Å)	V (Å <sup>3</sup> )	Z	rV(F,{E3})(Å <sup>3</sup> )		
Crystal [2]	4.2188	4.2188	6.9912	124.43	2	17.8		
DFT-ELF	4.2346	4.2346	7.1942	129.0	2	18.4		
<i>Interatomic distances (Å) - 1) crystal - 2) ab initio relaxed geom.. and ELF analyses</i>								
1)	Xe-F	1.999	Xe-Ftp	3.338	F-Ftp	3.025	Ftp high	2.994
	Xe-E	0.99	F-E	2.23	Ftp-E	2.82		
2)	Xe-F	2.078	Xe-Ftp	3.358	F-Ftp	3.046	Ftp high	3.039
	Xe-Ec	0.98	Xe-E	0.93	Ec-E	0.05	E ellipsoid a/b/c	0.70/0.70/0.92
	F-Ec	2.30	Ftp-E	2.84				
	>.T.<	1.40	∅Text	3.30	rEgyr	0.93	T.rd.rect. L/H/R	3.3/1.8/0.9

> T <: E torus diameter in median plane containing the three lone pairs. ∅Text and rTgir: E torus external diameter and gyration radius. T.rd.rect.: torus rounded rectangle encapsulating E torus section generated by E<sub>3</sub> revolving around Xe.

Ftp: fluorines making the tetragonal prism around Kr atom. Ftp high: high of tetragonal prism.

rE = (a.b.c)<sup>1/3</sup> = 0.77Å: average sphere of influence radius of each lone pair.

Table 4 - Molecular calculations on linear molecules NgF<sub>2</sub>.

Distances are in Å and frequencies in cm<sup>-1</sup>.

	d <sub>Ng-F</sub>	v <sub>F-Ng-F</sub> IR/bending	v <sub>F-Ng-F</sub> Ram./sym- stretching	v <sub>F-Ng-F</sub> IR/antisym -stretching
KrF <sub>2</sub>	1.93	216.93	470.10	573.00
XeF <sub>2</sub>	2.06	189.57	463.36	523.92
RnF <sub>2</sub>	2.18	163.41	450.30	488.10

## Figure Captions

**Figure 1.** The extended octet on Kr (10 electrons) in  $\text{KrF}_2$  Lewis structure (the same stands for  $\text{XeF}_2$ ). The three non bonding electron doublets are shown in color.

**Figure 2.** The two forms of tetragonal  $\text{KrF}_2$   $\alpha$  and  $\beta$  highlighting the different orientations of the linear F-Kr-F molecular entity. Kr atom is represented by deep blue circle with the associated three lone pairs.

**Figure 3.** a) Schematic perspective view of  $\alpha$   $\text{M}^*\text{F}_2\text{E}_3$  ( $\text{M}^* = \text{Kr}$  or  $\text{Xe}$ ) tetragonal crystal structure; the linear molecule F- $\text{M}^*$ -F is enclosed in a bicapped tetragonal prism  $\{\text{F}_2\text{Ftp}_8\}$  ( $\text{Ftp}_8 = \text{Ftp}_{\text{abcdefgh}}$ ). b) The three lone pairs  $\{\text{E}_3\}$  are represented according to Andersson's proposal [27]

**Figure 4 –** a) and b) ELF of  $\alpha$  and  $\beta$   $\text{KrF}_2$  difluorides: 3D (grey volumes) and 2D (slices). **a)**  $\alpha$ - $\text{KrF}_2\text{E}_3$ . Iso-values for 3D ELF at 0.854; **b)**  $\beta$   $\text{KrF}_2\text{E}_3$ . Iso-values for 3D ELF at 0.8556

**Figure 5 -** ELF 2D data sections: a) perpendicular to F-Kr-F molecule showing the median plane of  $\{\text{E}_3\}$  torus; b) in (110) plane, exhibiting the circular torus section (same diameter at  $90^\circ$ ) and its elliptic section of E electronic cloud associated to Ec. This section is well enclosed in a rounded rectangle (red line). Around F atom two symmetric density spots (with markedly lower density than Ec) are seen, defining the section of the ring of F electrons, underlined by a blue pale rounded rectangle ( $L = 1.37\text{\AA}$ ,  $H = 0.37\text{\AA}$ ). Worth noting the symmetric evolution of the two F electron clouds with  $\{\text{KrE}_3\}$  torus showing their interdependence.

**Figure 6 -**  $\alpha$ - and  $\beta$ -  $\text{KrF}_2\text{E}_3$  crystal structure aligned along [001]. The three lone pairs ( $\text{E}_3$ ) revolving around Kr leave a trace schematized by a pale blue torus. These representations show that in both cases cell volumes are somewhat filled by electronic densities.

**Figure 7 –** Projection onto (001) plane of the  $\text{KrF}_2\text{E}_3$  linear molecule. In this plane the fluorine atoms Fmnop pertaining to neighbor cell are indicated and apart the fluorine atoms Fabcd. The octahedra  $\text{F}_2\text{Fabcd}$ , Fa(FFopF)Fd and Fb(FFmnF)Fc are design and tilted on right part of the figure. The rounded rectangle (blue surface) shows the projection of  $\{\text{E}_3\}$  torus (exact scale) showing how important contribution in crystal architecture it brings.

**Figure 8 -** Cross sections of  $\beta$ - $\text{KrF}_2\text{E}_3$  ELF data: a) Section by  $(1\bar{1}0)$  plane showing a view along  $\{\text{KrE}_3\}$  torus axis and its deformation into an elliptic shape; b) Section by (001) plane at  $z = 1/2$  of  $\text{KrF}_2\text{E}_3$  molecule giving torus large deformation along [110] direction. Important to note that the F electron torus shape follows exactly the elliptic movement of  $\{\text{E}_3\}$  around Kr extreme values  $L = 1.46\text{\AA}$  and  $1.22\text{\AA}$  with a thickness  $H = 0.30\text{\AA}$ ; shows similar expansion

than in  $\alpha$  form ( $L = 1.37\text{\AA}$ ,  $H = 0.37\text{\AA}$ ) therefore with various extreme values like in the median plane torus.

**Figure 9** – Proposed mechanism for the phase transition  $\beta \rightarrow \alpha$   $\text{KrF}_2\text{E}_3$ :

- a)  $\beta$   $\text{KrF}_2$  linear molecules, alternatively localized in (001) planes in  $z = 0$  and  $1/2$ , remain parallel in each layer to  $(1\bar{1}0)$  or  $(110)$  planes. Molecules of neighboring cells participating by their fluorine Fmnp are indicated to show that the proposed mechanism can be seen directly within a unique cell;
- b)  $\text{KrF}_2\text{E}_3$  molecules of the cell can rotate in their own planes clockwise in layers  $z = 0$  and  $1$  and anticlockwise in the others;
- c) After  $90^\circ$  rotation the  $\alpha$   $\text{KrF}_2\text{E}_3$  phase is obtained.

**Figure 10** –  $\text{KrF}_2$ : Energy-volume curves for the two varieties and Birch EOS fits values in the insert.

**Figure 11** –  $\alpha$  and  $\beta$ - $\text{KrF}_2$ : Electronic band structures and site and orbital projections of the density of states.

**Figure 12** -  $\text{XeF}_2$ : 3D ELF envelops around F-Xe-F linear molecule in the body centered tetragonal structure highlighting the  $E_3$  triplet revolution around Xe and the driving of F electronic cloud marked by its enlargement shell in perpendicular direction to F-Xe-F linear molecule.

**Figure 13**- Electron localization sections in ELF  $\text{XeF}_2$  data. a) perpendicular to F-Xe-F molecule direction; b) in  $(110)$  plane, showing clearly the elliptic torus section. Figure 13- Electron localization sections in ELF  $\text{XeF}_2$  data. a) Perpendicular to F-Xe-F molecule direction; b) in  $(110)$  plane, showing clearly the elliptic torus section. Around F atom two symmetric density spots alike in Kr  $\alpha$  form (with markedly lower density than Ec its IDC  $\approx 0.84$ ) are seen which are defining the section of the ring of F electrons swept by the large torus center of “dynamic” {E3}. They are underlined by a blue pale rounded rectangle ( $L = 1.39\text{\AA}$ ,  $H = 0.30\text{\AA}$ ) therefore slightly repulsed away from F center by  $0.1\text{\AA}$ .



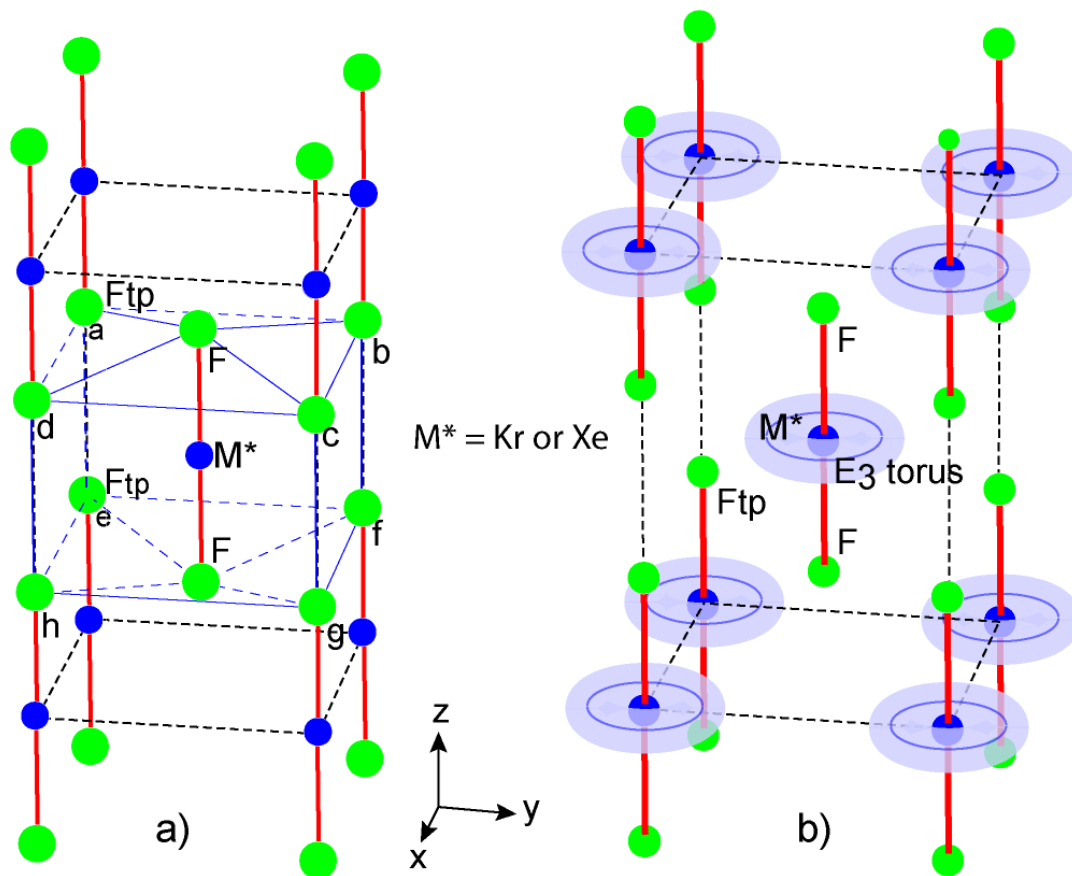
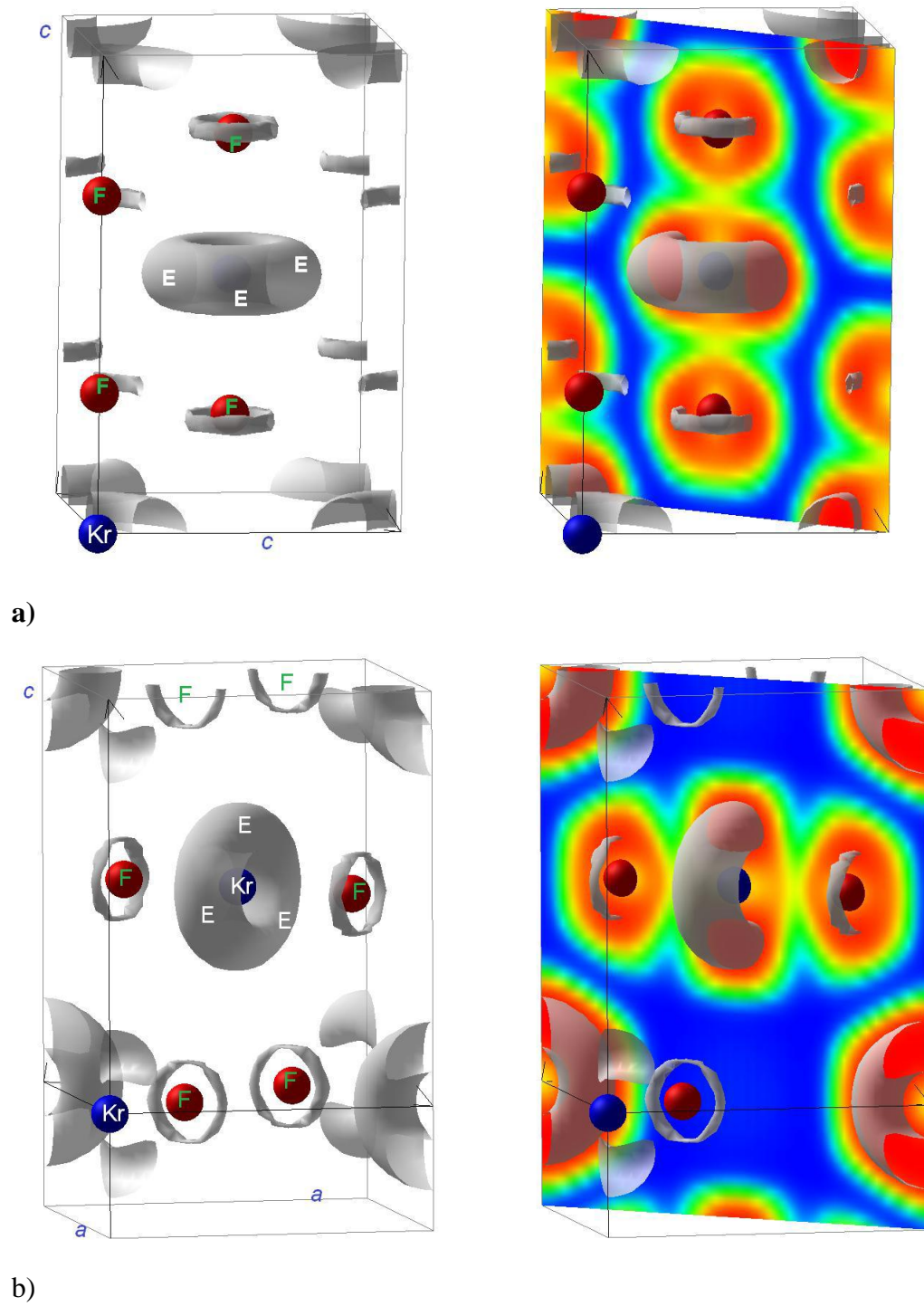


Figure 3



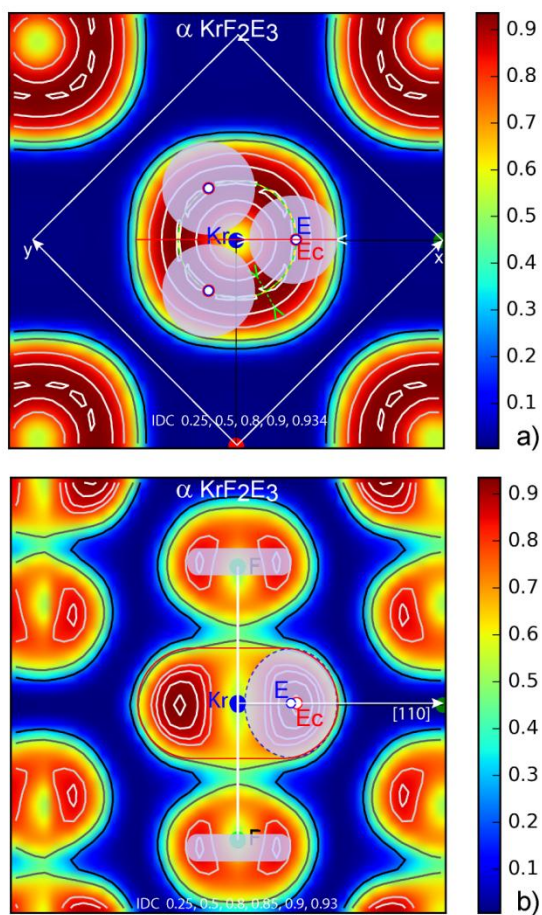


Figure 5

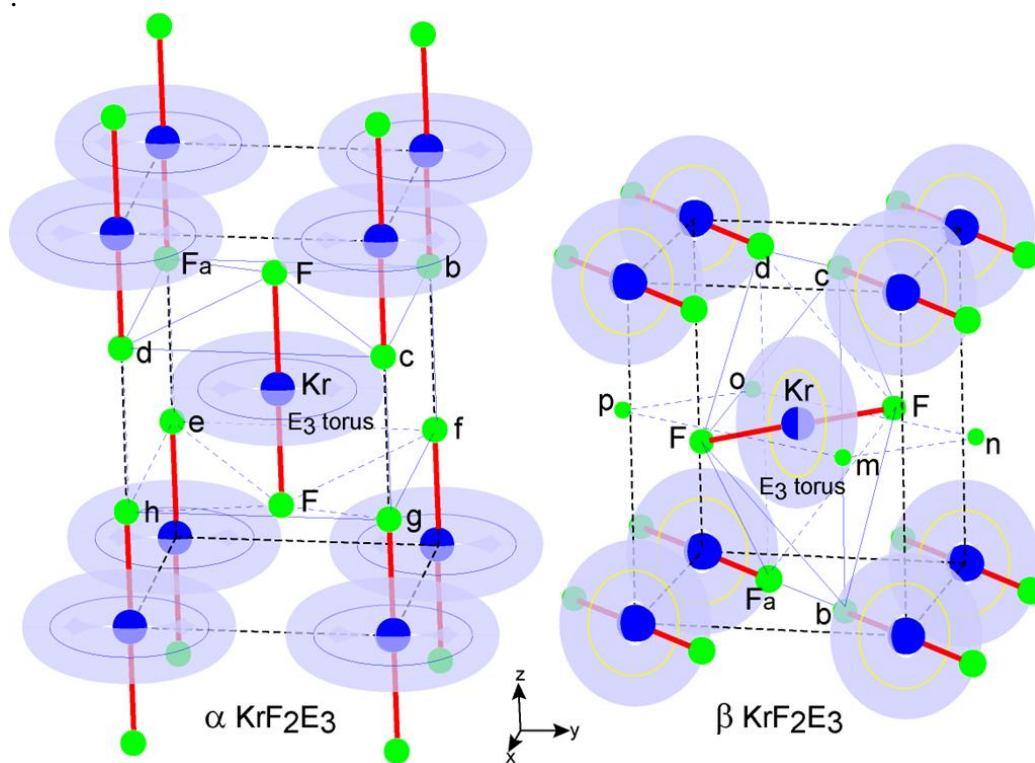


Figure 6

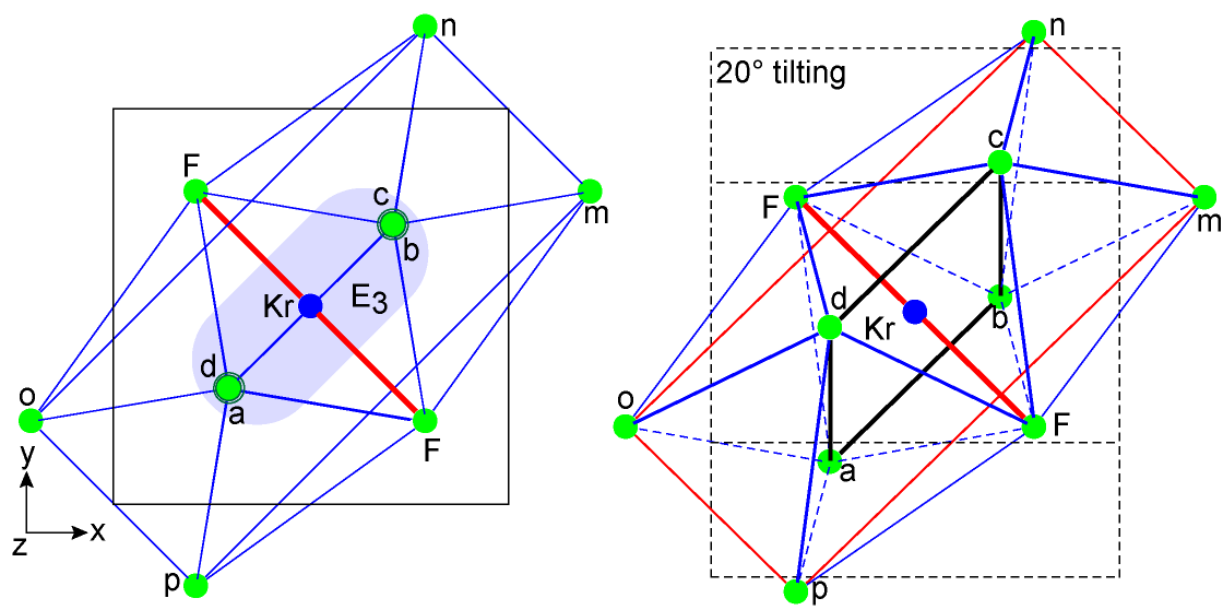


Figure 7

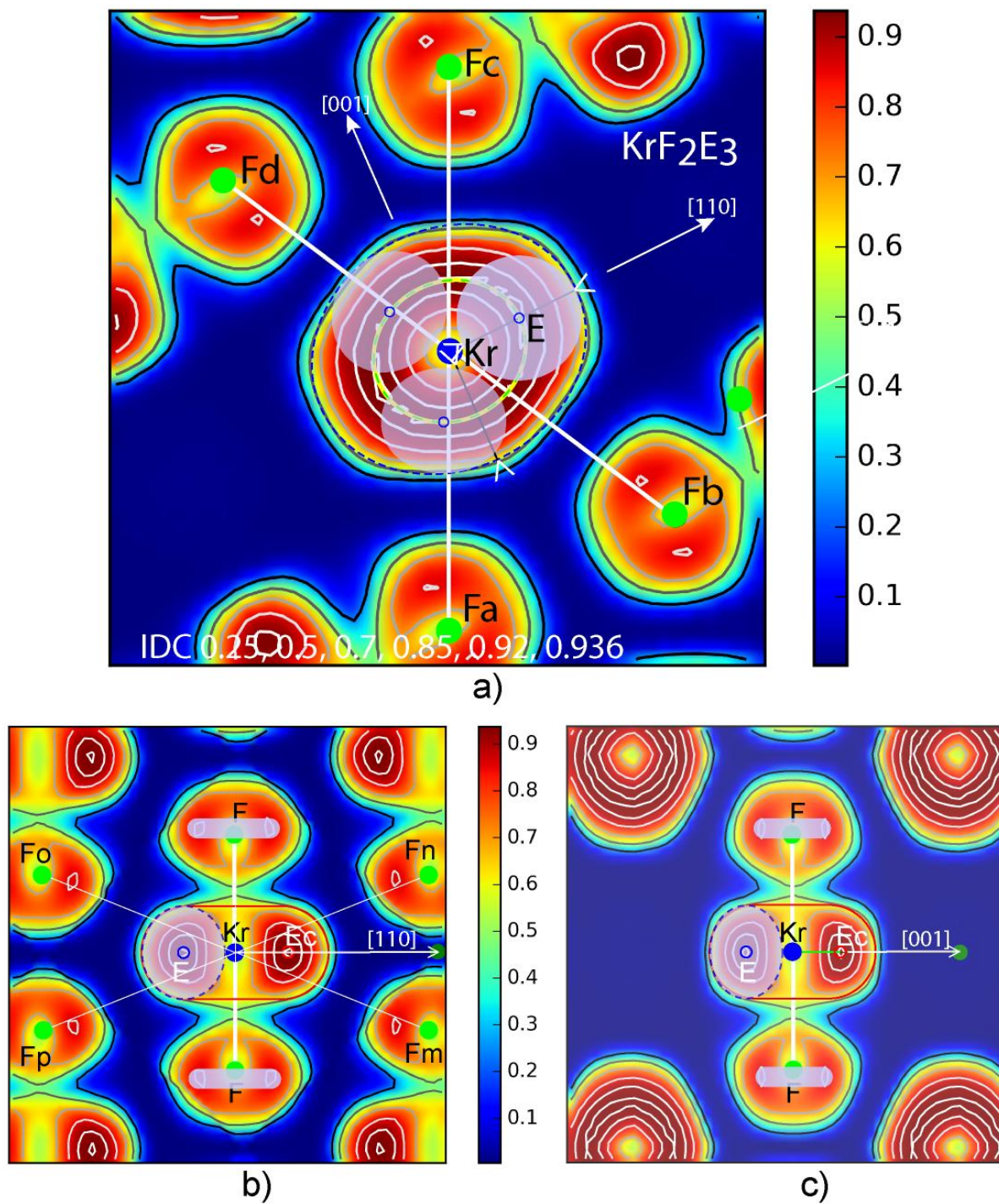


Figure 8.

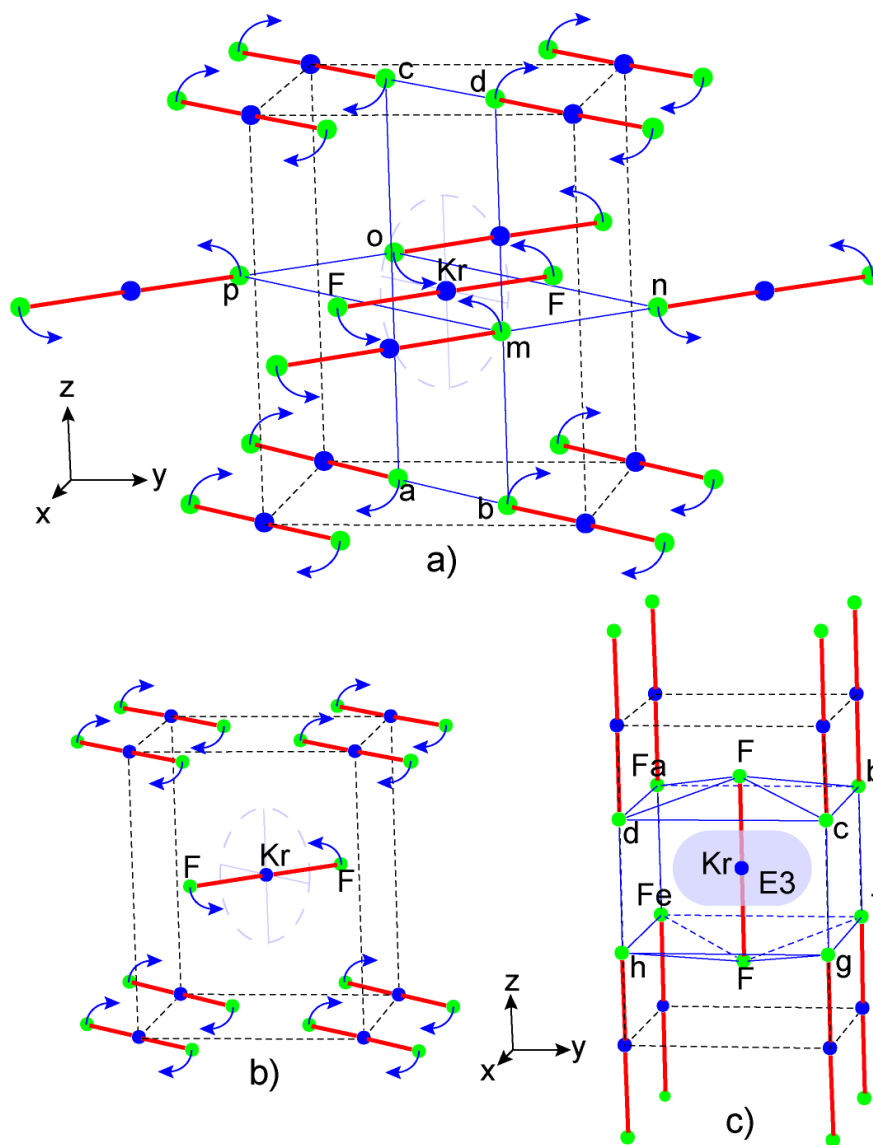


Figure 9.

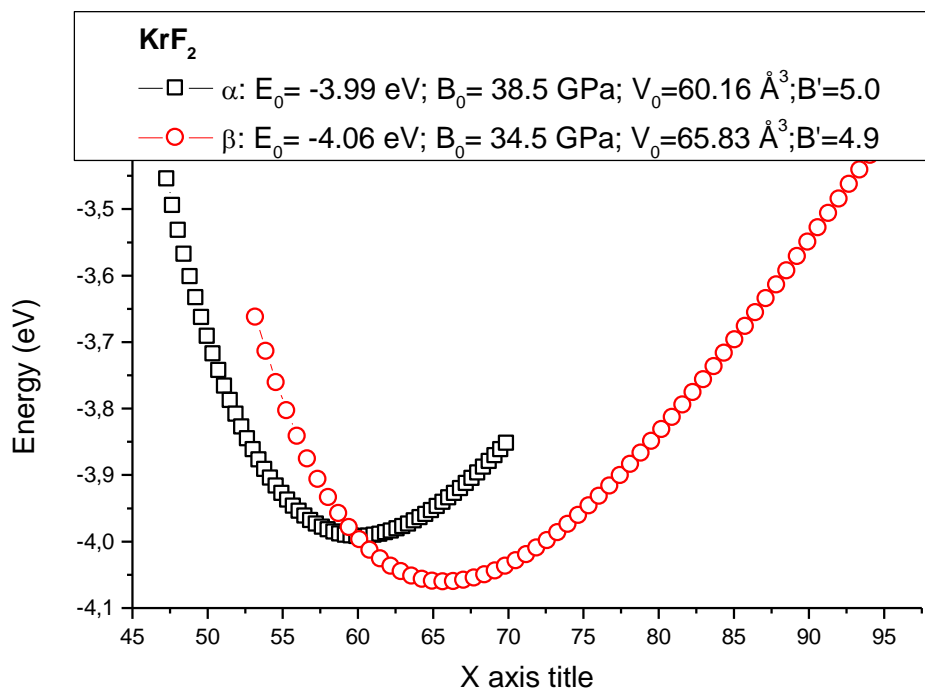


Figure 10

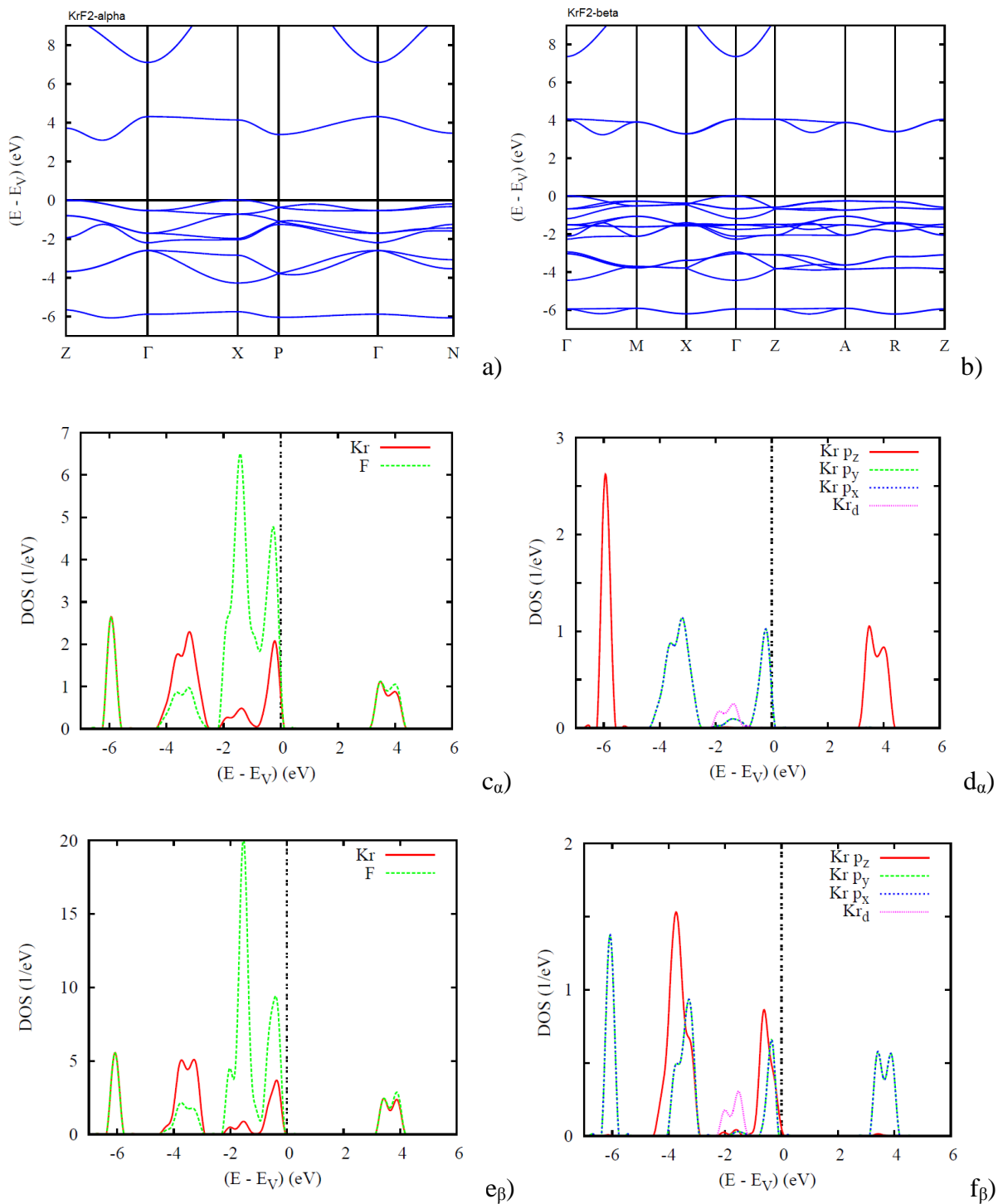
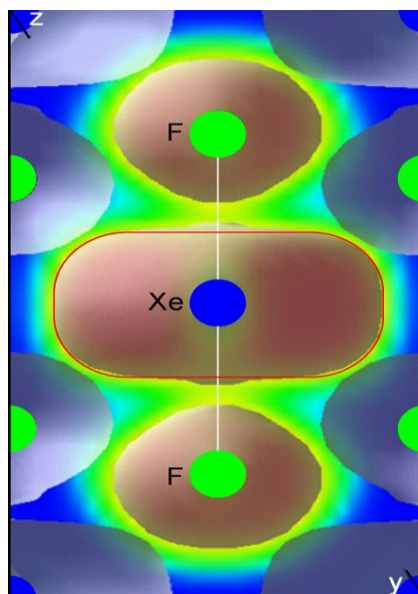


Figure 11.



**Figure 12**

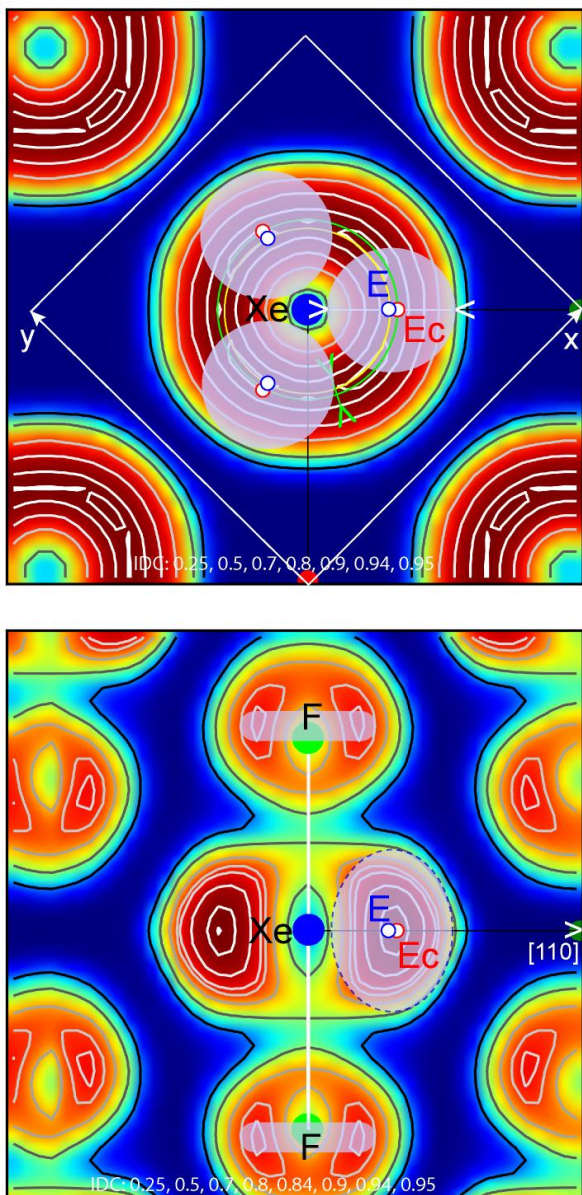


Figure 13